

Lawrence Berkeley National Laboratory

LBL Publications

Title

Neutron-unbound excited states of N23

Permalink

<https://escholarship.org/uc/item/7pq15973>

Journal

Physical Review C, 95(4)

ISSN

2469-9985

Authors

Jones, MD

Baumann, T

Brett, J

et al.

Publication Date

2017-04-01

DOI

10.1103/physrevc.95.044323

Peer reviewed

Neutron-unbound excited states of ^{23}N

M. D. Jones,^{1,2,*} T. Baumann,¹ J. Brett,³ J. Bullaro,⁴ P. A. DeYoung,³ J. E. Finck,⁵ N. Frank,⁴ K. Hammerton,^{1,6} J. Hinnefeld,⁷ Z. Kohley,^{1,6} A. N. Kuchera,¹ J. Pereira,¹ A. Rabeh,⁴ J. K. Smith,^{1,2,†} A. Spyrou,^{1,2} S. L. Stephenson,⁸ K. Stiefel,^{1,6} M. Tuttle-Timm,⁴ R. G. T. Zegers,^{1,2,9} and M. Thoennessen^{1,2}

¹National Superconducting Cyclotron Laboratory, Michigan State University, East Lansing, Michigan 48824, USA

²Department of Physics and Astronomy, Michigan State University, East Lansing, Michigan 48824, USA

³Department of Physics, Hope College, Holland, Michigan 49422-9000, USA

⁴Department of Physics and Astronomy, Augustana College, Rock Island, Illinois 61201, USA

⁵Department of Physics, Central Michigan University, Mount Pleasant, Michigan 48859, USA

⁶Department of Chemistry, Michigan State University, East Lansing, Michigan 48824, USA

⁷Department of Physics and Astronomy, Indiana University South Bend, South Bend, Indiana 46634-7111, USA

⁸Department of Physics, Gettysburg College, Gettysburg, Pennsylvania 17325, USA

⁹Joint Institute for Nuclear Astrophysics – Center for the Evolution of the Elements, Michigan State University, East Lansing, Michigan 48824, USA

(Received 22 July 2016; revised manuscript received 3 March 2017; published 25 April 2017)

Neutron unbound states in ^{23}N were populated via proton knockout from an 83.4 MeV/nucleon ^{24}O beam on a liquid deuterium target. The two-body decay energy displays two peaks at $E_1 \sim 100$ keV and $E_2 \sim 1$ MeV with respect to the neutron separation energy. The data are consistent with shell model calculations predicting resonances at excitation energies of ~ 3.6 MeV and ~ 4.5 MeV. The selectivity of the reaction implies that these states correspond to the first and second $3/2^-$ states. The energy of the first state is about 1.3 MeV lower than the first excited 2^+ in ^{24}O . This decrease is largely due to coupling with the $\pi p_{3/2}^{-1}$ hole along with a small reduction of the $N = 16$ shell gap in ^{23}N .

DOI: [10.1103/PhysRevC.95.044323](https://doi.org/10.1103/PhysRevC.95.044323)

I. INTRODUCTION

Spectroscopy of nuclei with extreme N/Z ratios can provide valuable insight into nuclear structure. Due to shifts in the single particle energies of exotic nuclei, classical shell closures can disappear while new shell gaps appear [1,2]. A well-known example of this is the “island of inversion,” located around $A \sim 32$, where a quenching of the $N = 20$ shell gap results in nuclei with ground states occupying the pf shell instead of the sd shell [3]. In the oxygen isotopes, there is substantial evidence for the breakdown of the $N = 20$ shell gap, and the appearance of $N = 16$ as a magic number [4–7]. This shift has been attributed to the tensor component of the NN interaction [8,9] as well as three-body forces [10].

As one moves down the $N = 16$ isotones, the removal of protons from the $\pi 0d_{5/2}$ orbital enables the $\nu 0d_{3/2}$ orbital to move higher in excitation resulting in a large energy difference between the $\nu 1s_{1/2}$ and $\nu 0d_{3/2}$ orbits in oxygen [2]. At present, there are no reports of bound- or unbound-excited states in the lighter isotones ^{23}N and ^{22}C . The measurement of these excited states can provide a better understanding of the changing shell structure in this region of the nuclear chart by extending our knowledge of the $N = 16$ gap into the proton p shell. In this article, we present first experimental information on neutron-unbound excited states in ^{23}N populated via proton-knockout from ^{24}O .

II. EXPERIMENTAL METHOD

The experiment was carried out at the National Superconducting Cyclotron Laboratory (NSCL) where a 140 MeV/nucleon ^{48}Ca beam impinged upon a ^9Be target with a thickness of 1363 mg/cm² to produce an ^{24}O beam at 83.4 MeV/nucleon. The A1900 fragment separator was used to select ^{24}O from the other fragmentation products, and the remaining beam contaminants were removed by time-of-flight in the off-line analysis. The ^{24}O beam proceeded to the experimental area where it impinged on the Ursinus College Liquid Hydrogen Target, filled with liquid deuterium (LD_2). Based on the design of Ryuto *et al.* [11], the LD_2 target is cylindrical with a diameter of 38 mm, a length of 30 mm, and is sealed with 125 μm -thick Kapton foils on each side.

A one-proton removal reaction from the ^{24}O beam created ^{23}N in an excited state above the neutron separation energy S_n , which promptly decayed to ^{22}N . The resulting charged fragments were then swept 43.3° by a 4-Tm superconducting sweeper magnet [12] into a collection of position- and energy-sensitive charged-particle detectors.

Element identification was achieved via a ΔE vs. time-of-flight measurement, and isotope identification was obtained through correlations in the time-of-flight, dispersive position, and dispersive angle following the sweeper magnet. Additional information on this procedure can be found in Ref. [13]. The position and momentum of the charged fragments at the target were reconstructed using an inverse transformation matrix, obtained from the program COSY INFINITY [14,15].

The neutrons emitted in the decay of ^{23}N traveled undisturbed by the magnetic field towards the Modular Neutron Array (MoNA) [16] and the Large-area multi-Institutional

*mdjones@lbl.gov; Present address: LBNL, Berkeley, CA 94720, USA.

†Present address: Reed College, 3203 SE Woodstock Blvd, Portland, Oregon 97202, USA.

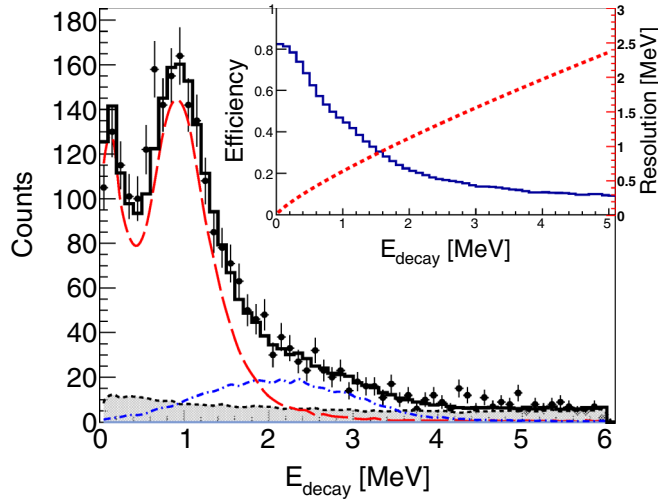


FIG. 1. Two-body decay energy for $^{22}\text{N} + 1n$. The best fit includes two-channel Breit-Wigners resulting from two states at 1.1 MeV (dashed-red line) and 2.4 MeV (dot-dashed-blue line). Background contributions are in shaded gray. The efficiency and resolution are shown in the inset as the blue histogram (left scale) and red-dashed line (right scale), respectively.

Scintillator Array (LISA). MoNA and LISA each consist of 144 bars of plastic scintillator with photomultiplier tubes on both ends and provide a measurement of neutron time-of-flight and position. Additional details on the experimental setup can be found in Refs. [17,18]. MoNA, LISA, and the sweeper provide a full kinematic measurement of the neutrons and charged particles emitted in the decay of ^{23}N .

III. ANALYSIS

The two-body decay energy is defined as

$$E_{\text{decay}} = M^* - M_{^{22}\text{N}} - m_n,$$

where M^* is the invariant mass of the decaying system, $M_{^{22}\text{N}}$ the mass of ^{22}N , and m_n the neutron mass. The decay energy, E_{decay} , corresponds to the excitation energy in ^{23}N above the neutron emission threshold. The invariant mass of the two-body system is obtained from the experimentally measured four-momenta of ^{22}N and the first time-ordered interaction in MoNA-LISA. To remove interactions from background γ rays, a time-of-flight gate on prompt neutrons in coincidence with ^{22}N fragments was applied. The observed two-body decay energy for ^{23}N is shown in Fig. 1, and displays two prominent peaks at $E_1 \sim 100$ keV and $E_2 \sim 1$ MeV. The efficiency and resolution of MoNA-LISA for the present setup are shown as a function of the decay energy in the inset.

A Monte Carlo simulation was used to model the decay of ^{23}N . The simulation includes the beam characteristics, the reaction mechanism, and subsequent decay. The efficiency, resolution, and acceptance of the charged particle detectors, along with the response of MoNA-LISA, are fully incorporated into the simulation. Therefore the results of the simulation are directly comparable to the experimental spectra. The neutron interactions in MoNA-LISA were modeled with

GEANT4 [19] and MENATE_R [20]. A modification was made to the $^{12}\text{C}(n,np)^{11}\text{B}$ inelastic cross section within MENATE_R to better agree with previous measurement [21] at $T_n = 90$ MeV. No qualitative change was observed in the shape of the simulated one-neutron decay energy spectrum when the inelastic cross sections for neutrons on carbon were increased or decreased by an order of magnitude in MENATE_R.

The input decay energy line shape was an energy dependent Breit-Wigner of the form

$$\sigma_l(E) \sim \frac{\Gamma_l}{(E_0 - E)^2 + \frac{1}{4}(\Gamma_l^2)},$$

where E_0 is the position of the peak and Γ_l the energy-dependent width. Given that ^{22}N has two bound excited states [22], it is possible for the neutron decay to branch to multiple final states. To model this, the two-channel form of the Breit-Wigner was used with a common normalization:

$$\sigma_{\text{tot}}(E) \sim \sigma_1(E; E_1) + \sigma_2(E; E_2),$$

where E_i is the energy of each branch, and the width in the numerator Γ_l becomes the partial-width Γ_i . The total widths Γ_i^T replace the width in the denominator and are given by the expressions

$$\Gamma_1^T = \Gamma_1(E) + \Gamma_2(E - E_{12}),$$

$$\Gamma_2^T = \Gamma_1(E + E_{12}) + \Gamma_2(E),$$

where $E_{12} = E_1 - E_2$ is the energy difference between the channels, with E_1 denoting the higher-energy channel. For simplicity, the shift functions have been neglected.

While it is possible for higher-lying states to be present at $E_{\text{decay}} > 3$ MeV, they are not resolved in the data and treated as background. Nonresonant contributions were modeled with a Gaussian decay distribution with a central energy of $E_{\text{decay}} = 10$ MeV and a width of $\sigma = 5$ MeV. This choice of line-shape reproduces the relative velocity between the fragment and neutron well and has been used to describe nonresonant contributions in the decay of ^{24}O , populated by knockout from ^{26}F [4].

The measured decay energy can be related to the excitation energy of ^{23}N by $E^* = E_{\text{decay}} + S_n$, where S_n was calculated using the mass excesses from Gaudefroy *et al.* [23]. Their values of $\Delta M_{^{23}\text{N}} = 36.72(0.28)$ MeV and $\Delta M_{^{22}\text{N}} = 31.11(0.26)$ MeV result in a one neutron separation energy of $S_n = 2.46(0.38)$ MeV. This separation energy is about 700 keV higher than what is obtained using the masses in the 2012 AME [24]. The two-neutron separation energy is $S_{2n} = 4.67(0.30)$ MeV.

Using the mass excesses measured by Gaudefroy *et al.* [23], theoretical predictions for the excited states of ^{23}N are shown in Fig. 2 with various interactions based on Ref. [25] including the WBP, WBT, WBTM, and WBM Hamiltonians in addition to the continuum shell model (CSM) [26]. The WBTM and WBM interactions contain a 12.5% and 25% reduction of the neutron-neutron interaction strength in the sd space. In the lighter nitrogen isotopes, a 12.5% reduction was necessary to reproduce the low-lying levels [22,27], while a 25% reduction was needed for the heavier carbon nuclei [22]. Proton excitations were limited to the p shell, while neutron

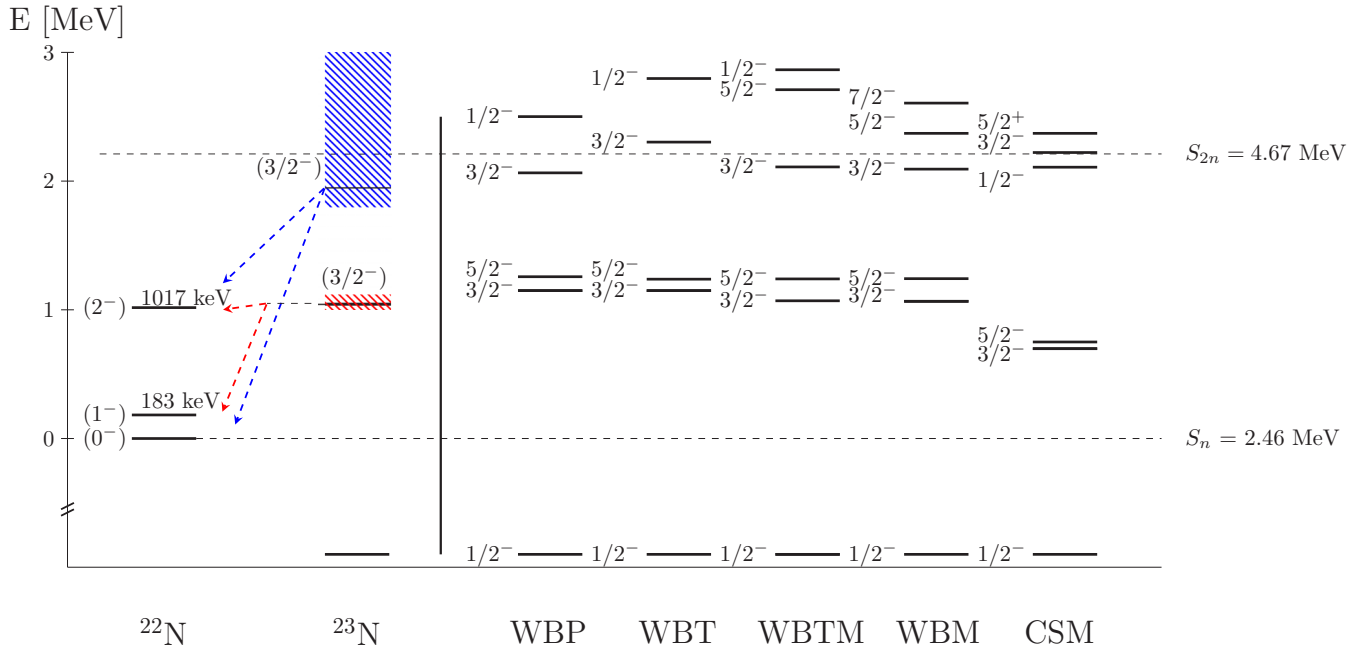


FIG. 2. A possible level ordering in ^{23}N consistent with the observed spectrum. The arrows indicate transitions from the first- and second-excited $3/2^-$ state in ^{23}N to various states in ^{22}N . The hatched areas indicate the experimental uncertainty given the assumptions discussed in the text. The colors correspond to the fit in Fig. 1. The branching from the $3/2^-$ states to the various excited states of ^{22}N cannot be resolved without γ detection. Shell model calculations for ^{23}N are shown for comparison on the right.

excitations were restricted to the sd shell. These calculations predict several excited states with spin-parity $1/2^-$, $3/2^-$, and $5/2^-$ in the vicinity of 3–5 MeV. Due to the selective nature of the proton removal reaction, it is not likely to populate a $5/2^-$ state in ^{23}N from ^{24}O . A $5/2^-$ state in ^{23}N can be made by coupling of the $p_{1/2}$ proton hole to the 2^+ state of the ^{24}O core, or by coupling of a $p_{3/2}$ proton hole to the 2^+ or 1^+ state in the ^{24}O core. The ground state of ^{24}O has very little to no overlap with these configurations in ^{23}N .

The spectroscopic overlaps C^2S between ^{23}N and ^{24}O were calculated using the WBP and WBT Hamiltonians in NUSHELLX [28] and are summarized in Table I. The largest overlap is with the ground state of ^{23}N , which is bound and was not within the acceptance of the sweeper magnet in this

TABLE I. Spectroscopic overlaps between various J^π in ^{23}N and the ground state of ^{24}O , calculated using the WBP and WBT interactions [25].

J^π	WBP		WBT	
	E_{calc} (MeV)	$\langle ^{23}\text{N} ^{24}\text{O} \rangle$ C^2S	E_{calc} (MeV)	$\langle ^{23}\text{N} ^{24}\text{O} \rangle$ C^2S
$1/2_1^-$	0	1.9328	0	1.9529
$1/2_2^-$	4.961	0.0025	5.257	0
$\sum C^2S$		1.9578		1.9529
$3/2_1^-$	3.610	1.4645	3.610	0.6893
$3/2_2^-$	4.525	0.6480	4.764	1.0483
$3/2_3^-$	5.215	0.1682	5.471	0.0944
$3/2_4^-$	6.989	1.4324	6.693	1.8889
$\sum C^2S$		3.7130		3.7209

experiment. The next strongest overlaps are for the $3/2^-$ states where the single-particle strength is fragmented. Given that the overlap for the first $1/2^-$ excited state is very small, the most likely candidate for the spin-parity of the observed state(s) is $3/2^-$.

It is important to note that ^{22}N has two bound excited states, one at 183 keV, and another at 1017 keV [22]. Although the spin-parities of these states are unknown, the tentative assignments of the ground, first, and second excited states are 0^- , 1^- , and 2^- , respectively. Thus, the observed peaks in the two-body decay energy could correspond to transitions to the 2^- excited state of ^{22}N instead of the ground state or the first excited 1^- state. Although there are neutron-unbound states in ^{22}N that ^{23}N could decay to, the selection of ^{22}N in the sweeper eliminates any contributions from these branches in the two-body spectrum of ^{23}N .

As it is not possible to discern between any number of degeneracies or level orderings that could produce the observed spectrum without measuring the emitted γ rays, one has to rely on theoretical calculations. For this reason, the data are interpreted and fit within the context of the shell-model predictions.

Of the interactions considered here, none predict a state near threshold (see Fig. 2). The lowest $3/2^-$ state is predicted to be at approximately 1 MeV above S_n , with the second $3/2^-$ being about an MeV higher. The 100 keV peak then does not correspond to a decay to the ground state but rather a transition to the 2^- state in ^{22}N , while the $E_2 \sim 1$ MeV peak is comprised of transitions to both the first-excited and ground state of ^{22}N . While there are three possible final states, the splitting between the ground and first-excited state cannot be resolved due to the experimental resolution for decay energies above 1 MeV. For

this reason, the 0^- and 1^- states are treated as a single state at their average energy. Since the spacing between the two $3/2^-$ states is expected to be about an MeV, another state was assumed to be around ~ 2 MeV. In addition, because the final states in ^{22}N are only tentatively known, the ℓ values are chosen to be consistent with the interpretation.

The assumption of a second excited state is qualitatively supported by the data, as the high-energy tail cannot be described without excessive widths. In order to fit the spectrum with a single two-channel Breit-Wigner, it is necessary for the 1 MeV peak to have $\ell = 2$ and a width of $\Gamma \sim 1.5$ MeV. In this scenario, it is also necessary for the 100 keV branch to be $\ell = 0$ as the relative intensity of the peaks is driven by the partial widths. The cross section for $\ell = 2$ drops rapidly as E_{decay} approaches zero and the 100 keV peak cannot be $\ell = 2$ in the presence of another broad channel unless it has an even larger width.

The spectrum can also not be described with both channels being $\ell = 0$, because the widths are coupled and the penetrability for $\ell = 0$ is constant. Thus, if the 1 MeV channel is made excessively broad so too is the 100 keV branch and the fit fails to describe the data.

The single-particle decay width for the decay to the ground state is 200 keV for $\ell = 2$. Examining the spectroscopic factors in Table I, we note that the $3/2^-$ single-particle strength is fragmented indicating that these states are mixed in their neutron configurations. Thus one would expect widths less than the single-particle width, and so the solution with a single state is neglected due to the large necessary width. The data are fit with two-channel Breit-Wigners resulting from two $3/2^-$ states separated by approximately 1 MeV.

Since the branching ratios are not constrained without the knowledge of the γ -ray decays in ^{22}N , there are too many free parameters to uniquely describe the data. Therefore a set of narrow widths was chosen to reduce the parameter space. These widths are $\Gamma_i = 150$ keV for the low-energy branches of the two states ($\ell = 0$) and 400 keV ($\ell = 0$) and 300 keV ($\ell = 2$) for the high-energy branch of the first and second $3/2^-$ states, respectively.

The energies of the two $3/2^-$ are then minimized simultaneously after fixing the partial widths. In addition, the energy of each branch is required to be consistent during the minimization. The best-fit energies for the two $3/2^-$ states are $E_{\text{decay}} = 1070 \pm 100$ keV, and $E_{\text{decay}} = 2500^{+500}_{-700}$ keV. The errors in the fit parameters are approximate due to the fixed partial widths. They are purely statistical and are determined by the 1σ limit in the χ^2 minimization. Accounting for the separation energy places the first excited $3/2^-$ at $E_x = 3530 \pm 100$ (stat) ± 400 (sys) keV.

At present the uncertainties are too large to uniquely determine the contributions from the possible branchings two $3/2^-$ states would produce. In order to completely disentangle the spectrum, one would need to measure the emitted γ rays in a triple-coincidence measurement ($n + \gamma + ^{22}\text{N}$).

IV. DISCUSSION

The present measurement alone is not sufficient to fully determine the size of the $N = 16$ shell gap in ^{23}N . In ^{24}O

the $N = 16$ shell gap was calculated by taking the $(2J + 1)$ weighted average of the 1^+ and 2^+ excited states, as they are composed of $1p-1h$ excitations above the ^{24}O ground state [4]. Similarly, the same can be done in ^{23}N , but one needs to take into account four states as the 2^+ and 1^+ configuration of neutrons, $(\nu 1s_{1/2})^1 \otimes (\nu 0d_{3/2})^1$, can couple with the unpaired $\pi 0p_{1/2}$ proton to give $(5/2^-, 3/2^-)$ and $(3/2^-, 1/2^-)$, respectively. The situation is further complicated by the fact that the $1p-1h$ neutron configuration in ^{23}N will mix with the $\pi 0p_{3/2}$ hole, lowering its energy.

In the WBP, WBT, WBTM, and WBM interactions, the lowest $3/2^-$ state in ^{23}N is indeed a mixture, with the occupation numbers giving a significant proton hole in the $\pi p_{1/2}$ and $\pi p_{3/2}$ orbitals, and a $(\nu 1s_{1/2})^1 \otimes (\nu 0d_{3/2})^1$ configuration of neutrons. One may write the wave function for the $3/2^-$ state as

$$|^{23}\text{N}\rangle_{3/2^-} = \alpha p_{3/2}^{-1} \otimes |^{24}\text{O}\rangle_{\text{g.s.}} + \beta p_{1/2}^{-1} \otimes |^{24}\text{O}\rangle_{2^+} + \gamma p_{1/2}^{-1} \otimes |^{24}\text{O}\rangle_{1^+},$$

where α , β , and γ are coefficients constrained by the normalization $\alpha^2 + \beta^2 + \gamma^2 = 1$. According to the WBP calculation, the pure $\pi p_{3/2}^{-1}$ configuration comprises of roughly 37% of the total wave function ($\alpha \sim 1/\sqrt{3}$), with the remaining amplitude shared equally between the 2^+ and 1^+ configurations.

Thus the energy of the lowest $3/2^-$ state depends on both the $N = 16$ shell gap and the energy of the $\pi 0p_{3/2}^{-1}$ hole, which is dictated by the spin-orbit splitting. The splitting between the $d_{3/2}-s_{1/2}$ and $p_{1/2}-p_{3/2}$ orbitals can be altered within NUSHELLX to study this dependence.

Let Δ denote the change in energy for either the $d_{3/2}$ or $p_{1/2}$ orbital for both protons and neutrons from their initial values in the WBP calculation, using the same model-space restrictions as before. Figure 3 shows the energy of the lowest $3/2^-$ state as

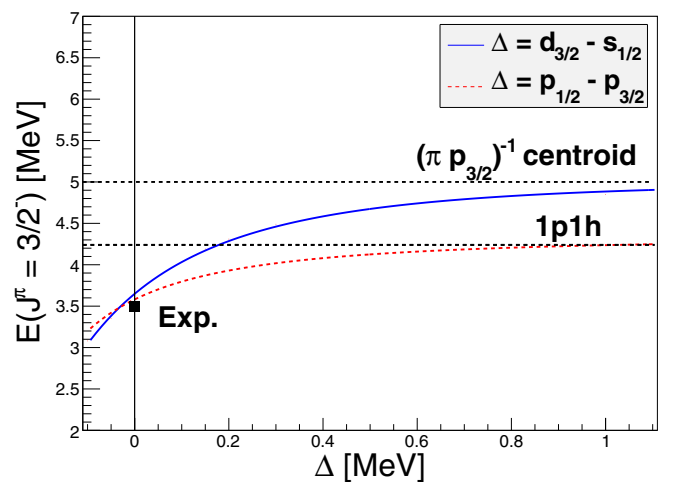


FIG. 3. Energy dependence of the first-excited $3/2^-$ state on the shift, Δ , on the energy of the $d_{3/2}$ orbital (solid-blue line) or $p_{1/2}$ orbit (dashed-red line). The dotted black lines denote the energies of the pure $1p-1h$ or $\pi p_{3/2}^{-1}$ configurations in the initial calculation ($\Delta = 0$). The experimental energy determined in this work is denoted by the black square.

a function of either the $N = 16$ shell gap (solid-blue line) or the spin-orbit splitting (dotted-red line). By increasing the energy of the $d_{3/2}$ or $p_{1/2}$ orbitals independently, the mixing between the configurations is reduced until they are separated at the asymptotes. In the case of the $d_{3/2}$ orbit, increasing the $N = 16$ shell gap causes the $1p-1h$ configuration to be prohibitively costly in energy thus the $3/2^-$ state is comprised entirely of the $\pi p_{3/2}^{-1}$ hole. Likewise, increasing the spin-orbit splitting causes the promotion of a particle from the $\pi p_{3/2}$ to the $\pi p_{1/2}$ to be too energetic, and the lower energy configuration is instead the $1p-1h$ configuration across the $N = 16$ shell gap.

Evidence for the size of the $N = 16$ shell gap in ^{24}O can be deduced from the energy of the first excited 2^+ state as shown in Figure 4 of Ref. [4]. In order to calculate the equivalent energy in ^{23}N one has to take the $(2J + 1)$ weighted average of the first $3/2^-$ and $5/2^-$ states. All Hamiltonians considered in Fig. 2 predict these two states to be nearly degenerate, thus the excitation energy of the $3/2^-$ measured in the present experiment can be used to estimate the equivalent 2^+ energy.

The most recent ENSDF evaluation lists the excitation energy of the first 2^+ in ^{24}O as 4.79(11) MeV [29], corresponding to the weighted average of 4.82(11) [4] and 4.75(14) [5]. A more recent measurement of 4.70(15) MeV [30] agrees with this evaluation.

The present value of the excitation energy of about 3.5 MeV for the $3/2^-$ state in ^{23}N is 1.3 MeV lower than the 2^+ state in ^{24}O . In the limit of no mixing from the $p_{3/2}^{-1}$ hole configuration, $[\Delta(p_{1/2}) \sim 1]$, the energy of the lowest $3/2^-$ increases from 3.61 MeV to 4.24 MeV which is 500 keV lower than the excitation of the 2^+ in ^{24}O . The $N = 16$ shell gap, or the $(2J + 1)$ average of the four lowest states in the $1p-1h$ multiplet, is around 4.53 MeV when the contributions from the $p_{3/2}^{-1}$ configuration are removed. This value is 300–400 keV lower than in ^{24}O where this average was found to be 4.95(16) MeV [4], thus the shell gap in ^{23}N is comparable to ^{24}O . The shift in the effective 2^+ energy is largely due to the coupling to the $p_{3/2}$ hole. In order to confirm this experimentally the excitation energy of the $5/2^-$ state in ^{23}N should be measured.

V. CONCLUSIONS

Neutron unbound excited states in ^{23}N were populated via proton knockout from an ^{24}O beam on a deuterium target. The two-body decay energy of ^{23}N displays two prominent peaks at $E_1 \sim 100$ keV and $E_2 \sim 1$ MeV. Because the daughter nuclide ^{22}N has two bound excited states, it is not possible to distinguish between degeneracies or multiple level schemes that may produce the observed energy differences in the two-body spectrum of ^{23}N . A triple coincidence experiment detecting the ^{22}N fragments, neutrons and γ rays is necessary to measure the branchings to the different final states.

The data are consistent with several shell model interactions which predict a $3/2^-$ state at ~ 1 MeV and ~ 2 MeV above S_n in ^{23}N . Similar to the first excited 2^+ state in ^{24}O , the first of these two $3/2^-$ states can be used to estimate the $N = 16$ shell gap. Its excitation energy of about 3.5 MeV is significantly lower than the ^{24}O 2^+ state at 4.8 MeV, however this reduction is largely due to configuration mixing with the $\pi p_{3/2}^{-1}$ hole, thus indicating only a slight a reduction of the $N = 16$ gap in nitrogen.

Finally, in order to compare these data directly it is necessary to measure the first excited $5/2^-$ state in ^{23}N . A future experiment designed to populate this state, for example inelastic excitation of ^{23}N , would be valuable. In addition, the distribution of single-particle strength for the $3/2^-$ will be vital to determining the $\pi p_{3/2}^{-1}$ centroid experimentally and further understanding the mixing between the $1p1h$ and $\pi p_{3/2}^{-1}$ configurations.

ACKNOWLEDGMENTS

We thank L. A. Riley for the use of the Ursinus College Liquid Hydrogen Target, and A. O. Macchiavelli for many thoughtful and useful discussions. This work was supported by the National Science Foundation under Grants No. PHY14-04236, PHY12-05537, PHY11-02511, PHY11-01745, PHY14-30152, PHY09-69058, and PHY12-05357. The material is also based upon work supported by the Department of Energy National Nuclear Security Administration under Award No. DE-NA0000979.

-
- [1] R. Kanungo, *Phys. Scr.* **T152**, 014002 (2013).
 [2] T. Otsuka, *Phys. Scr.* **T152**, 014007 (2013).
 [3] E. K. Warburton, J. A. Becker, and B. A. Brown, *Phys. Rev. C* **41**, 1147 (1990).
 [4] C. Hoffman, T. Baumann, D. Bazin, J. Brown, G. Christian, D. Denby, P. DeYoung, J. Finck, N. Frank, J. Hinnefeld, S. Mosby, W. Peters, W. Rogers, A. Schiller, A. Spyrou, M. Scott, S. Tabor, M. Thoennessen, and P. Voss, *Phys. Lett. B* **672**, 17 (2009).
 [5] K. Tshoo, Y. Satou, H. Bhang, S. Choi, T. Nakamura, Y. Kondo, S. Deguchi, Y. Kawada, N. Kobayashi, Y. Nakayama, K. N. Tanaka, N. Tanaka, N. Aoi, M. Ishihara, T. Motobayashi, H. Otsu, H. Sakurai, S. Takeuchi, Y. Togano, K. Yoneda, Z. H. Li, F. Delaunay, J. Gibelin, F. M. Marqués, N. A. Orr, T. Honda, M. Matsushita, T. Kobayashi, Y. Miyashita, T. Sumikama, K. Yoshinaga, S. Shimoura, D. Sohler, T. Zheng, and Z. X. Cao, *Phys. Rev. Lett.* **109**, 022501 (2012).
 [6] R. Kanungo, C. Nociforo, A. Prochazka, T. Aumann, D. Boutin, D. Cortina-Gil, B. Davids, M. Diakaki, F. Farinon, H. Geissel, R. Gernhäuser, J. Gerl, R. Janik, B. Jonson, B. Kindler, R. Knöbel, R. Krücken, M. Lantz, H. Lenske, Y. Litvinov, B. Lommel, K. Mahata, P. Maierbeck, A. Musumarra, T. Nilsson, T. Otsuka, C. Perro, C. Scheidenberger, B. Sitar, P. Strmen, B. Sun, I. Szarka, I. Tanihata, Y. Utsuno, H. Weick, and M. Winkler, *Phys. Rev. Lett.* **102**, 152501 (2009).
 [7] T. Baumann, A. Spyrou, and M. Thoennessen, *Rep. Prog. Phys.* **75**, 036301 (2012).
 [8] T. Otsuka, T. Suzuki, R. Fujimoto, H. Grawe, and Y. Akaishi, *Phys. Rev. Lett.* **95**, 232502 (2005).

- [9] T. Otsuka, T. Suzuki, M. Honma, Y. Utsuno, N. Tsunoda, K. Tsukiyama, and M. Hjorth-Jensen, *Phys. Rev. Lett.* **104**, 012501 (2010).
- [10] T. Otsuka, T. Suzuki, J. D. Holt, A. Schwenk, and Y. Akaishi, *Phys. Rev. Lett.* **105**, 032501 (2010).
- [11] H. Ryuto, M. Kunibu, T. Minemura, T. Motobayashi, K. Sagara, S. Shimoura, M. Tamaki, Y. Yanagisawa, and Y. Yano, *Nucl. Instrum. Methods Phys. Res. A* **555**, 1 (2005).
- [12] M. Bird *et al.*, *IEEE Trans. Appl. Supercond.* **15**, 1252 (2005).
- [13] G. Christian, N. Frank, S. Ash, T. Baumann, P. A. DeYoung, J. E. Finck, A. Gade, G. F. Grinyer, B. Luther, M. Mosby, S. Mosby, J. K. Smith, J. Snyder, A. Spyrou, M. J. Strongman, M. Thoennessen, M. Warren, D. Weisshaar, and A. Wersal, *Phys. Rev. C* **85**, 034327 (2012).
- [14] N. Frank, A. Schiller, D. Bazin, W. Peters, and M. Thoennessen, *Nucl. Instrum. Methods Phys. Res. A* **580**, 1478 (2007).
- [15] K. Makino and M. Berz, *Nucl. Instrum. Methods Phys. Res. A* **558**, 346 (2006).
- [16] B. Luther *et al.*, *Nucl. Instrum. Methods Phys. Res. A* **505**, 33 (2003).
- [17] M. D. Jones, N. Frank, T. Baumann, J. Brett, J. Bullaro, P. A. DeYoung, J. E. Finck, K. Hammerton, J. Hinnefeld, Z. Kohley, A. N. Kuchera, J. Pereira, A. Rabeh, W. F. Rogers, J. K. Smith, A. Spyrou, S. L. Stephenson, K. Stiefel, M. Tuttle-Timm, R. G. T. Zegers, and M. Thoennessen, *Phys. Rev. C* **92**, 051306(R) (2015).
- [18] M. D. Jones, Ph.D. thesis, Michigan State University, 2015.
- [19] S. Agostinelli *et al.*, *Nucl. Instrum. Methods Phys. Res. A* **506**, 250 (2003).
- [20] B. Roeder, Development and validation of neutron detection simulations for EURISOL, EURISOL Design Study, Report No. 10-25-2008-006-In-beamvalidations.pdf (2008), p. 31, http://ns.ph.liv.ac.uk/eurisol/M3_in-beam_validations.pdf.
- [21] D. A. Kellogg, *Phys. Rev.* **90**, 224 (1953).
- [22] D. Sohler, M. Stanoiu, Z. Dombrádi, F. Azaiez, B. A. Brown, M. G. Saint-Laurent, O. Sorlin, Y.-E. Penionzhkevich, N. L. Achouri, J. C. Angélique, M. Belleguic, C. Borcea, C. Bourgeois, J. M. Daugas, F. De Oliveira-Santos, Z. Dlouhy, C. Donzaud, J. Duprat, Z. Elekes, S. Grévy, D. Guillemaud-Mueller, F. Ibrahim, S. Leenhardt, M. Lewitowicz, M. J. Lopez-Jimenez, S. M. Lukyanov, W. Mittig, J. Mrázek, F. Negoita, Z. Podolyák, M. G. Porquet, F. Pougheon, P. Roussel-Chomaz, H. Savajols, G. Sletten, Y. Sobolev, C. Stodel, and J. Timár, *Phys. Rev. C* **77**, 044303 (2008).
- [23] L. Gaodefroy, W. Mittig, N. A. Orr, S. Varet, M. Chartier, P. Roussel-Chomaz, J. P. Ebran, B. Fernández-Domínguez, G. Frémont, P. Gangnant, A. Gillibert, S. Grévy, J. F. Libin, V. A. Maslov, S. Paschalis, B. Pietras, Y.-E. Penionzhkevich, C. Spitaels, and A. C. C. Villari, *Phys. Rev. Lett.* **109**, 202503 (2012).
- [24] M. Wang, G. Audi, A. Wapstra, F. Kondev, M. MacCormick, X. Xu, and B. Pfeiffer, *Chin. Phys. C* **36**, 1603 (2012).
- [25] E. K. Warburton and B. A. Brown, *Phys. Rev. C* **46**, 923 (1992).
- [26] A. Volya and V. Zelevinsky, *Phys. Rev. C* **74**, 064314 (2006).
- [27] M. J. Strongman, A. Spyrou, C. R. Hoffman, T. Baumann, D. Bazin, J. Brown, P. A. DeYoung, J. E. Finck, N. Frank, S. Mosby, W. F. Rogers, G. F. Peaslee, W. A. Peters, A. Schiller, S. L. Tabor, and M. Thoennessen, *Phys. Rev. C* **80**, 021302(R) (2009).
- [28] B. Brown and W. Rae, *Nucl. Data Sheets* **120**, 115 (2014).
- [29] B. Singh, Evaluated Nuclear Structure Data Files (ENSDF) (2015).
- [30] W. F. Rogers, S. Garrett, A. Grovom, R. E. Anthony, A. Aulie, A. Barker, T. Baumann, J. J. Brett, J. Brown, G. Christian, P. A. DeYoung, J. E. Finck, N. Frank, A. Hamann, R. A. Haring-Kaye, J. Hinnefeld, A. R. Howe, N. T. Islam, M. D. Jones, A. N. Kuchera, J. Kwiatkowski, E. M. Lunderberg, B. Luther, D. A. Meyer, S. Mosby, A. Palmisano, R. Parkhurst, A. Peters, J. Smith, J. Snyder, A. Spyrou, S. L. Stephenson, M. Strongman, B. Sutherland, N. E. Taylor, and M. Thoennessen, *Phys. Rev. C* **92**, 034316 (2015).